Application Note 60

Timing and Recombination Unit (TRU) for Time-Resolved Spectroscopy and Multiphoton Microscopy

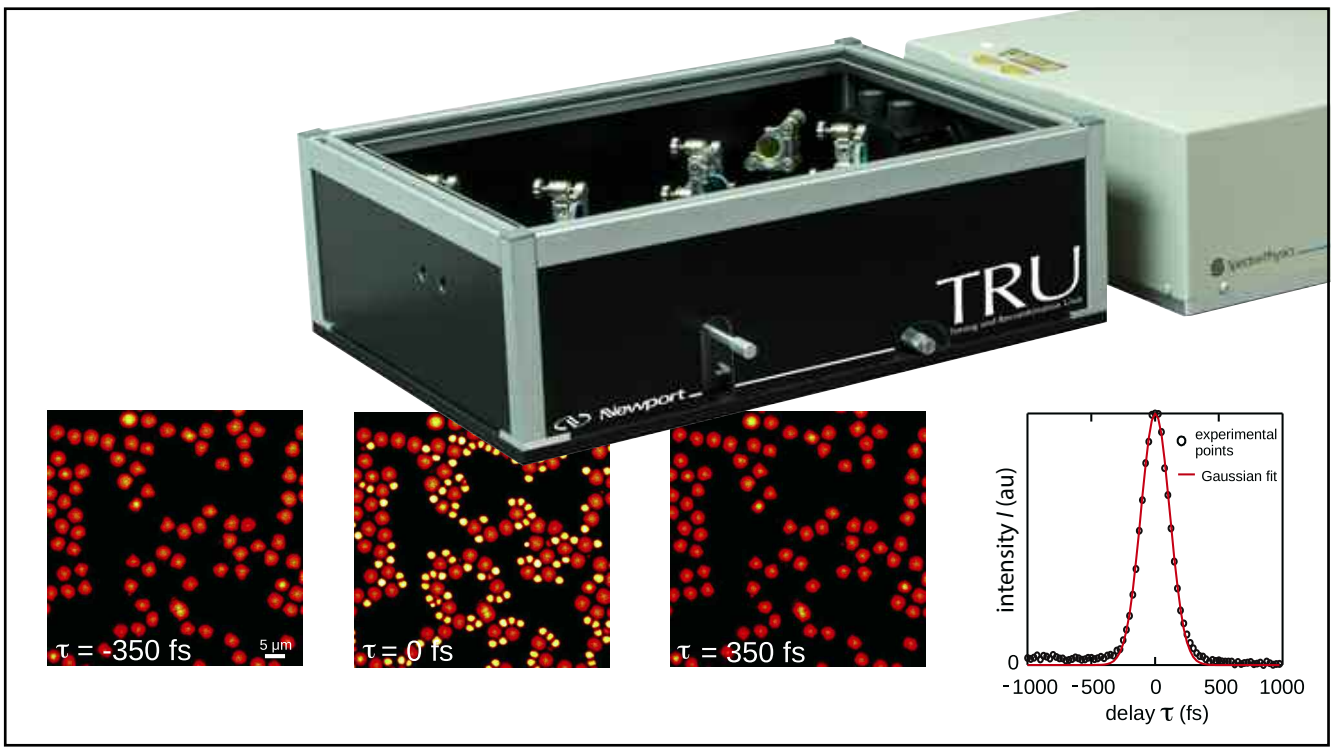

Newport
Experience | Solutions

Timing and Recombination Unit (TRU) for Time-Resolved Spectroscopy and Multiphoton Microscopy

1 Introduction

Recent market introduction of dual beam tunable lasers, such as Spectra-Physics InSight® DS+™ Dual, enable a variety of pump-probe and multiphoton microscopy techniques. These experiments require the two outputs of the laser to be synchronized in time, have well-defined beam paths (collinear or parallel), adjustable power and divergence. The Spectra-Physics InSight DS+ features 680 – 1300 nm gap-free tuning from a single source, nearly double the tuning range of Ti-Sapphire ultrafast lasers. In particular, the InSight DS+ delivers high average and peak power levels at long infrared wavelengths (>1 µm) for deepest in vivo imaging. With an integrated DeepSee™ dispersion pre-compensator, short sub-100 fs pulses are optimally delivered through a microscope to the specimen for maximum fluorescence and penetration depth. InSight DS+ also has exceptional beam pointing stability, beam quality and output power stability, as well as fast wavelength tuning, making it ideal for microscopy. When equipped with the dual output beam option, InSight DS+ Dual fully supports the diverse needs of multimodal imaging.

In this application note, we describe the Timing and Recombination Unit (TRU), a specially designed addition to dual wavelength, dual output laser sources, such as the Spectra-Physics InSight DS+ Dual, allowing the temporal overlap and independent beam conditioning of the two outputs. To demonstrate the performance of the TRU, we present the results of several pump-probe and multiphoton microscopy imaging experiments.

2 TRU: features and applications

The TRU is designed to synchronize the two output beams of dual output laser sources, such as the InSight DS+ Dual, facilitating a large variety of single and dual beam, ultrafast spectroscopy and imaging applications, such as single- and multi-color two-photon fluorescence (TPF), pump-probe, second harmonic generation (SHG), third harmonic generation (THG), stimulated Raman scattering (SRS), coherent anti-Stokes Raman scattering (CARS), and others.

Figure 1 shows the TRU (cover removed) with the InSight DS+ Dual laser. Inside the TRU box, each beam is conveniently equipped with a Newport VA-BB-4 manual ultrafast variable attenuator for precise power control of the transmitted output. A specially designed, high accuracy, dual position manual slider assembly allows switching from a single to a dual beam collinear setup without affecting alignment. In the single beam regime, both the fixed (1041 nm) and/or tunable (680 – 1300 nm) beams of InSight DS+ Dual are separately available. In the dual beam, collinear regime, it is possible to select the tunable laser wavelength from 760 nm to 940 nm, which when overlapped with the fixed 1041 nm output, corresponds to a Raman shift range of 1000 – 3500 cm^{-1} for CARS and SRS. This range is limited by the dichroic beamsplitter used to recombine the beams, and the geometry of the optical layout. The beam paths and variable delay line are optimized to temporally and spatially overlap the fixed and tunable beams. The TRU compensates for the optical delay introduced by downstream optics and the DeepSee pre-compressor inside the laser, ensuring that transform-limited pulses arrive at the focal plane of the objective. The system includes silver mirrors throughout, but the tunable output can be upgraded to broadband, ultrafast dielectric mirrors for higher throughput (see Table 1). Both versions provide temporally and spectrally distortion-free outputs.

3 Experiment

To demonstrate the performance and feasibility of TRU, we present results of experiments using pump-probe spectroscopy, as well as TPF, CARS, and THG imaging methods. This device can also be used for FRET and uncaging experiments, which are not discussed in this application note.

Fig. 1. TRU (cover removed) with the Spectra-Physics InSight DS+ Dual laser.

Table 1 – TRU Specifications

Fixed beam wavelength (typical)	1041 nm
Tunable beam spectral range (single beam)	680 – 1300 nm
Tunable beam spectral range (dual beam)	760 – 940 nm
Raman shift for CARS, SRS	1000 – 3500 cm^{-1}
Maximum throughput (dielectric mirrors option)	>85%
Maximum throughput (silver mirrors)	>70%
Attenuation of tunable and fixed beams	0 – 2 OD
Output polarization of tunable and fixed beams	S- (vertical) standard*
Beam entrance/exit height	4.75 in (120.65 mm)
Dimensions (L x W x H)	24 x 18 x 7.75 in {61 x 45.7 x 19.7 cm}

* TRU *can be custom configured for horizontal* P- *or mixed* S-/P- *outputs.*

3.1 Pump-probe measurements on SESAM

First, we show the performance of the TRU in the non-collinear dual beam configuration by carrying out pump-probe measurements on a semiconductor saturable absorber mirror (SESAM) sample. SESAM is a mirror structure with an incorporated semiconductor saturable absorber, commonly used for passive mode-locking of various types of lasers [1]. In the pump-probe method, a pump pulse excites the specimen, and a probe pulse is used for probing the specimen after an adjustable delay time. In particular, the method can be used to measure the recovery of the reflectivity of a SESAM after its excitation.

Figure 2(a) shows the sketch of our pump-probe experimental setup. The two beams delivered by the Spectra-Physics InSight DS+ Dual laser are exiting the TRU in a parallel non-collinear configuration. The tunable beam is passing through a chopper (Newport 3502) and a computer-controlled delay line (Newport 443 + LTA-HS + SMC100CC) and is used to pump the specimen. The use of an external delay line can in principle be avoided, since the second, fixed-wavelength beam is also passing through a delay line inside the TRU, but in this series of experiments we kept the position of the internal delay stage fixed for simultaneous experiments with collinear-beam configuration. The fixed beam at 1041 nm is used to probe the specimen. The two beams are focused together on the surface of the SESAM through an achromatic lens with 150 mm focal length and 50 mm diameter (Newport PAC21AR.16). The typical powers of the pump and probe beams at the specimen position input are 100 mW each. The

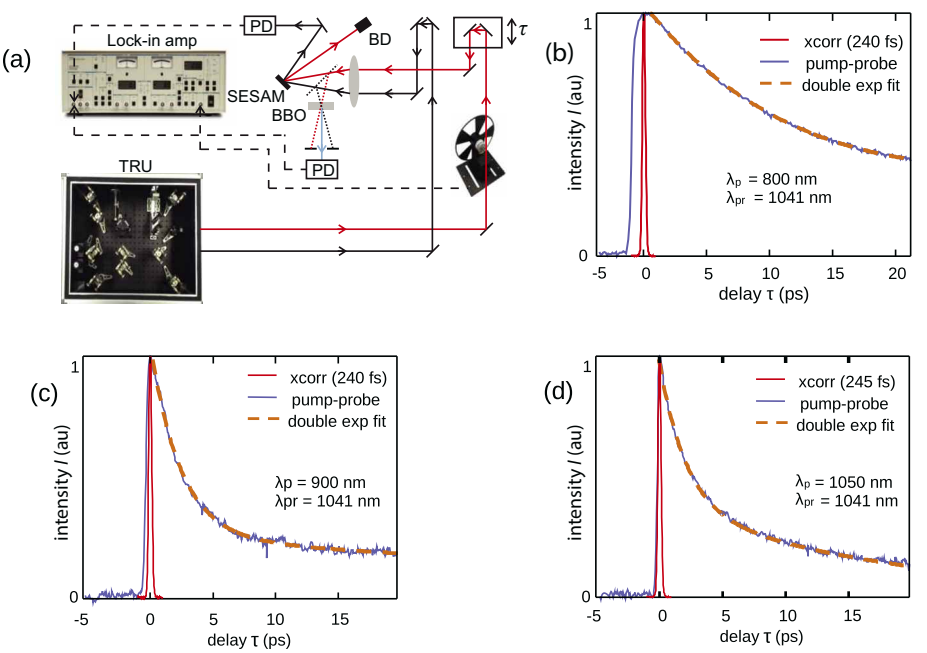

Fig. 2. Pump-probe measurements: (a) experimental setup, (b) $\lambda_p = 800\ nm$, $\tau_1 = 13.6\ ps$, $\tau_2 = 28\ ps$, *(c)* $\lambda_p = 900\ nm$, $\tau_1 = 2.4\ ps$, $\tau_2 = 66.5\ ps$, *(d)* $\lambda_p = 1050\ nm$, $\tau_1 = 2.1\ ps$, $\tau_2 = 19.6\ ps$.

reflected pump beam is blocked with a beam dump (BD), while the modulated probe beam is sent to an amplified photodetector (PD, Newport 818-BB-21A), which has a bandpass filter centered at 1040 nm attached to it. The signal is detected with a computer-controlled lock-in amplifier. To measure the instrument response function of the system, the two beams can be picked with a flip mirror after the lens and before the SESAM and sent to a nonlinear crystal (BBO) to generate the sum-frequency signal. The resulting signal, which is the cross-correlation of the pump and the probe pulses, is measured through the same procedure. The results of the pump-probe measurements are illustrated in Fig. 2(b – d). The reflectivity dynamics of the SESAM are shown for three different pump wavelengths λ_p = 800 nm (b), 900 nm (c), and 1050 nm (d), and the probe wavelength λ_{pr} = 1041 nm. The blue curves are the actual pump-probe measurements, the red curves are the cross-correlation measurements, and the dashed orange curves are bi-exponential fits. The cross-correlation durations are ~240 fs in all three cases. As expected, the data shows bi-exponential reflectance recovery. The fast component is due to quick intraband carrier relaxation, while the slow component describes the interband dynamics. The measured time constants τ_1 and τ_2 for Fig. 2(b – d) are as follows: τ_1 = 13.6 ps, τ_2 = 28 ps (b), τ_1 = 2.4 ps, τ_2 = 66.5 ps (c), τ_1 = 2.1 ps, τ_2 = 19.6 ps (d).

3.2 Two-color TPF imaging of polystyrene beads

Next, we carry out single- and two-color TPF imaging experiments in the collinear beam configuration of TRU. Single-color (degenerate) TPF microscopy enables 3D imaging of complex media at a cellular level deep within scattering tissue [2]. Although any single fluorescent dye can generally be observed using degenerate TPF microscopy, current methods do not provide simultaneous, efficient and independent two-photon excitation of more than two spectrally distinct fluorophores. On the other hand, two-color (non-degenerate) two-photon excitation of a fluorophore with two laser beams may offer independent degrees of freedom by tuning the power and wavelength of each beam [3]. The non-degenerate TPF imaging mechanism takes advantage of the infrared wavelengths used in three-photon microscopy [4] for increased penetration depth, while preserving relatively high two-photon excitation cross section, thus combining the advantages of both imaging techniques.

In our two-color TPF imaging experiments, the two beams from the Spectra-Physics InSight DS+ Dual laser are passing through the TRU where they are recombined in space and in time. One of the beams is tunable in the range of 760 – 940 nm, allowing to optimize both the single- and two-color TPF signals. The other beam is fixed at 1041 nm. Note that for single-color TPF the laser wavelength can be tuned in the range of 680 – 1300 nm. The two collinear beams exiting the TRU are coupled together into an upright microscope and focused on the specimen with a water immersion objective (25x, 1.05 NA). The powers of the beams at the microscope input are 5 mW for the fixed beam, and 20 μW for the tunable beam. TPF signals are collected in the epi direction at a pixel dwell time of 12.5 μs, resulting in 3.3 s of scan time for each frame. The collected images have 63.5 × 63.5 μm^2 size. A band-pass filter centered at 580 nm, along with short-pass filters to filter out the fundamental beams, are used before the PMT to filter out the TPF signals. The specimen is a mix of yellow-green (YG) and yellow-orange (YO) fluorescent polystyrene beads with 2 μm and 4.5 μm diameters, respectively. The wavelength of the tunable beam was set to 850 nm for brightest non-degenerate TPF imaging of the chosen fluorescent beads. The results of the TPF imaging experiments are summarized in Fig. 3. Figures 3 (a – c) show the non-degenerate TPF images at different time delays between the two beam: τ = –350 fs (a), τ = 350 fs (b), and τ = 0 fs (c). When the two pulses are not temporally overlapped, only the degenerate TPF from the 4.5 μm YO polystyrene beads is observed (a,b). This is due to the two-photon interaction from the 1041 nm fixed beam (as checked by blocking the tunable beam). The non-roundness of the beads is because of their deformation after the water in the solution has dried up. At time zero (c), the non-degenerate TPF signal from the 2 μm YG polystyrene beads is also activated. Figure 3(d) shows the instrument response function of this experiment (open circles), measured by targeting one of the YG polystyrene beads and changing the time delay by 25 fs steps. The FWHM duration of the Gaussian fit (red curve) is 265 fs.

The video of this time-dependent non-degenerate TPF signal can be viewed at **https://youtu.be/qsAbweZORq4.**

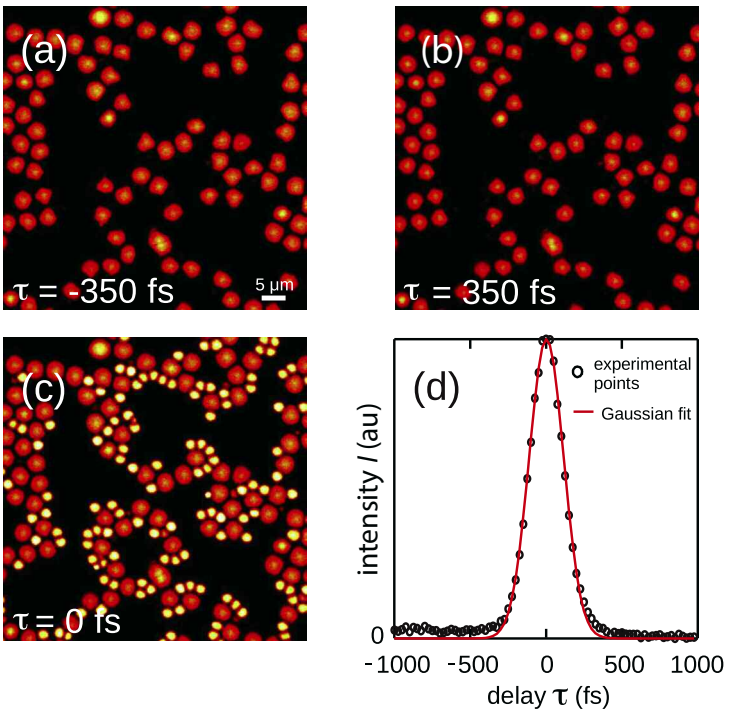

Fig. 3. Two-color (non-degenerate) TPF imaging of a mix of YG *and* YO *fluorescent polystyrene beads: (a – c) TPF images at different time delays between the two beams,* τ = –350 *fs,* τ = 350 *fs, and* τ= 0 *fs, (d) measured instrument response function of the experiment (open circles) with a Gaussian fit (red curve),* Δt = 265 *fs.*

3.3 CARS imaging of fiber

Next, we carry out CARS imaging experiments in the collinear beam configuration of TRU. CARS is a third-order nonlinear optical process where a pump-probe beam at the frequency ω_p and a Stokes beam at the frequency ω_S interact with molecules in the specimen [5,6]. When the difference frequency ω_p- ω_S is in resonance with a given molecular vibrational mode Ω, an anti-Stokes signal is generated at the frequency of ω_{aS}=2 ω_p- ω_S. Microscopy based on the CARS process is an imaging technology with applications in biology and medicine, allowing for noninvasive imaging of complex systems with high spatial resolution, high sensitivity, and label-free chemical specificity.

The schematic of the CARS imaging experiment is similar to the one for TPF imaging. The two collinear beams at λ_p = 800 nm and λ_S = 1041 nm exiting the TRU, recombined spatially and temporally, are coupled together into the microscope and focused on the specimen with a water immersion objective (25x, 1.05 NA). The powers of the pump and Stokes beams at the microscope input are 10 mW each, and the microscope throughput is 57% and 49% at 800 nm and 1041 nm, respectively. CARS signals are collected in the forward direction at a pixel dwell time of 20μs, resulting in 5.2 s of scan time for each frame. The collected images have 254 × 254 μm^2 size. Combination of short- and band-pass filters are used to filter out the CARS signal at 650 nm. As an imaging specimen we chose a piece of SMF-28 fiber (with coating) attached to a microscope slide. We put a drop of water directly on top of the microscope slide, thus immersing the fiber in water. The fiber consists of four layers: the dual-layer acrylate coating with an outer diameter of 245 ± 5 μm, the cladding with an outer diameter of 125 ± 0.7 μm, and the core with a diameter of 8.2 μm (see the schematic diagram of the SMF-28 fiber's cross section in the inset of Fig. 5(b)).

The results of the CARS imaging experiments are summarized in Fig. 4. Figure 4(a) shows the *z*-stack frame images of SMF-28 at $z = -20$ μm, $z = 0$ μm, and $z = 20$ μm, with z values going from negative to positive by moving the objective down (closer to the specimen). The *z*-stack imaging of the fiber is acquired with a Δz = 0.5 μm step size, making sure that the focal plane is passing from the fiber coating to its cladding. When the beams are focused inside the coating, bright CARS signal at 650 nm is observed due to the 3000 cm^{-1} Raman peak of the acrylate coating. Moving the focal plane into the glass cladding results in vanishing of the CARS signal, thus making it possible to detect the coating-cladding interface. The ImageJ software analysis of the *z*-stack is shown in Fig. 4(b). Here, the integrated CARS signals from the regions of interest, shown with red lines on the frames of Fig. 4(a), are plotted versus the depth z (open circles). The solid lines in Fig. 4(b) are high-order polynomial fits to the measurements. Moving the focal plane from the fiber coating into the cladding results in a signal decrease from 800 counts to <200 counts, which is at the level of the PMT dark counts. To check the repeatability of the method, the same measurement is done at two different starting *z* positions by shifting the objective 4 μm (red and blue curves). To find the interface between the fiber coating and cladding, we calculate the derivatives of the polynomials on Fig. 4(b) and fit them with Gaussian functions. The calculated derivatives are depicted in Fig. 4(c) with red and blue curves, together with the Gaussian fits (dashed black).

The two Gaussian fits $A=A_0 e^{-\left(\frac{z-z_0}{\Delta z}\right)^2}$ have the following coefficients: z_0^r = 1μm, Δz^r = 4 μm, z_0^b = −3.1μm, Δz^b = 4 μm, where z_0 is the peak position, and Δz is the width at 1/*e* level. The difference between the peak positions is $z_0^r - z_0^b$ = 4.1 μm, in good agreement with the 4 μm shift of the objective position between the measurements. The widths of the Gaussian fits are 4 μm in both cases, showing that the interface between the fiber coating and cladding can be determined with 4 μm accuracy. Next, from the fiber specs we know that the cladding diameter of SMF-28 is 125 ± 0.7 μm, so taking into account the spherical aberration caused by the fiber curvature it will be possible to find the center of the fiber core by moving the objective down.

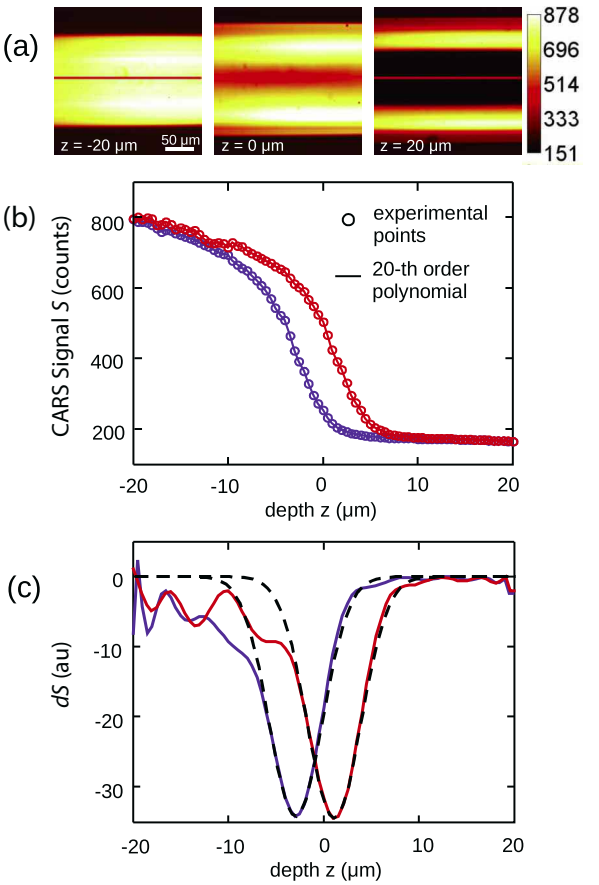

Fig. 4. CARS imaging of SMF-28 fiber: (a) z-stack images at z = −20 μm, z = 0 μm, and z = 20 μm, red lines indicate the region of interest, (b) CARS signal versus z, (c) derivative of the CARS signal versus z.

3.4 THG imaging of fiber

We then image the SMF-28 fiber by another multiphoton microscopy technique - THG imaging. THG microscopy is a non-fluorescent multiphoton technique that combines the advantages of label-free imaging with restriction of signal generation to the focal spot of the scanning laser [7,8]. THG imaging is especially suited for the three-dimensional imaging of transparent specimens. It is either generated near gradients in the refractive index or in the third-order nonlinear susceptibility $X^{(3)}$. Since it has a third-order dependence on the excitation intensity, it is generated primarily in the focal region, automatically resulting in sectioned imaging. It is a background-free imaging technique requiring no additional staining. The long excitation wavelength (>1μm), in combination with the non-resonant nature of the THG process, makes the technique potentially non-bleaching and further minimizes possible biological damage.

To carry out THG imaging measurements, we switch from the dual beam collinear configuration of TRU to the single beam setup. This allows accessing the entire tuning range of the laser (680-1300 nm). In the initial series of experiments, the beam at λ= 1200 nm exiting the TRU is coupled into the microscope and focused on the specimen. The power at the microscope input is 250 mW, and the microscope throughput is ~20% at 1200 nm. THG signals at 400 nm are collected both in the forward and epi directions at a pixel dwell time of 8 μs, resulting in 2.1 s of scan time for each frame. The collected images have 254 × 254 μm^2 size.

Figure 5 summarizes the results of the THG imaging experiments when the signals are collected in the forward scattering direction. The z-stack images are acquired in the range of z = −5 μm to z = 255 μm with a Δz = 1 μm step size, making sure that the focal plane is passing from top to bottom of the fiber. Figure 5(a) shows the z-stack images at z = 4 μm, z = 34 μm, and z = 65 μm. The **ImageJ** analysis of the z-stack is shown in Fig. 5(b), where the background associated with the PMT dark counts is subtracted: six peaks are observed during the scan, corresponding to different interfaces inside the fiber. The first three peaks in Fig. 5(b) correspond to the THG signal generation from the water-coating layer 1, coating layer 1-coating layer 2 (the SMF-28 has a dual acrylate coating), and coating layer 2-cladding interfaces, respectively, and the last three weaker peaks (zoomed inset) correspond to the THG signal generation from the interfaces in the inverted order. Similar to the fiber imaging results shown in [8], in our experiments the cladding-core interface is also not resolved (Fig. 5). This we attribute to the fact that the imaging setup in this experiment is limited in signal-to-noise – the effective dynamic range is given by a maximum signal count of ~4000 against ~200 dark count noise from the detection system. The schematic diagram of the SMF-28 fiber's cross section according to its specs is shown in the inset of Fig. 5(b). The interface positions found by the THG imaging are matching perfectly with the actual positions for the first three peaks (z = 4 μm, 34 μm, 65 μm), while the other three peaks are shifted significantly (>10 μm). This we attribute to the lens formation (spherical aberration) inside the fiber due to its curvature. The other inset of Fig. 5(b) shows the YZ orthogonal view of the fiber processed by **ImageJ**, in good visual agreement with the schematic diagram. To measure the accuracy of our measurements, we again fit the first three peaks with Gaussian functions (red, blue and orange dashed lines).The widths of these fits are as follows: Δz^r = 2.2 μm, Δz^b = 2.2 μm, Δz^o = 3.6 μm, which yields that the water-coating layer 1, coating layer 1-coating layer 2 interfaces can be found with 2.2 μm accuracy, and the coating layer 2-cladding interface can be found with 3.6 μm accuracy, which is close to the 4 μm value measured with the CARS imaging technique. Experiments on THG imaging in the epi direction show similar results with ~2 times weaker THG signals.

THG images of the fiber are also acquired by tuning the laser wavelength to 1050 nm. In this series of experiments, the forward detection channel of the microscope is modified for the detection of the THG wavelength at 350 nm. The *z*-stack images are acquired in the range of $z = -20$ μm to $z = 20$ μm with a Δz = 0.5 μm step size, making sure that the focal plane is passing from the coating to the cladding of the fiber. The results are illustrated in Fig. 6. Figure 6(a) shows the *z*-stack images at $z = -2$ μm, $z = 4$ μm, and $z = 10$ μm. Figure 6(b) shows the THG signal versus the depth *z*. The width of the Gaussian fit (red curve) is Δz = 3.5 μm, in good agreement with the values measured with the CARS imaging technique and the THG imaging at 1200 nm.

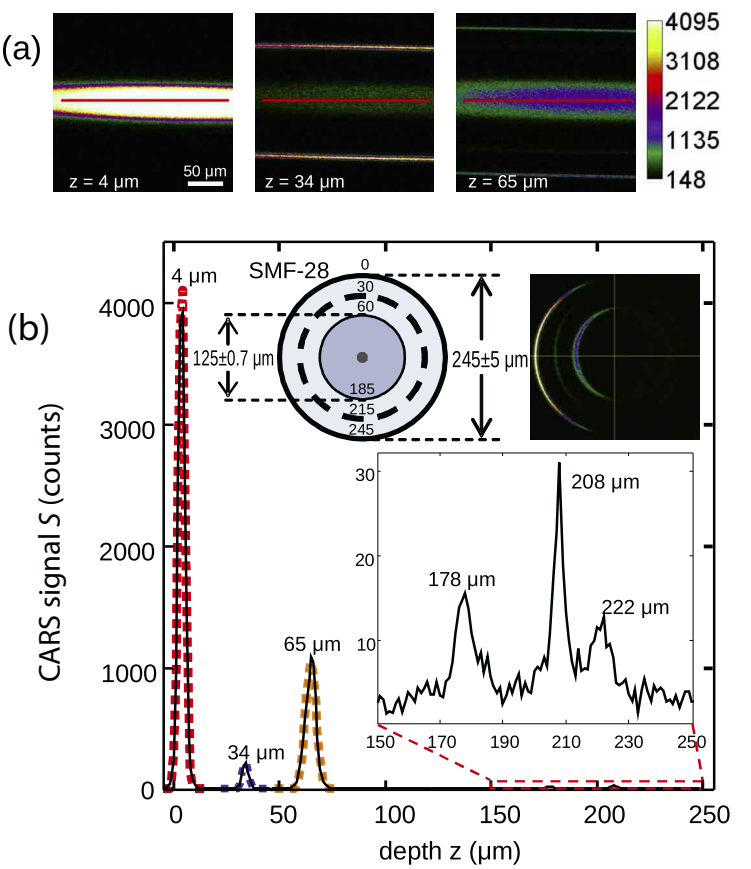

Fig. 5. THG imaging of SMF-28 fiber with 1200 nm excitation: (a) z-stack images at z = 4 μm, z = 34 μm, and z = 65 μm, (b) CARS signal versus z, insets show the schematic diagram and the YZ orthogonal view of the fiber cross section.

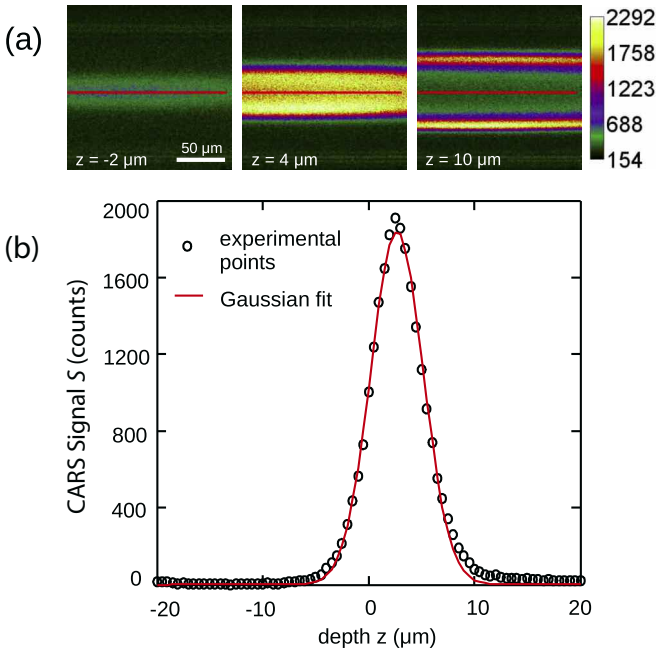

Fig. 6. THG imaging of SMF-28 fiber with 1050 nm excitation: (a) z-stack images at z = –2 µm, z = 4 µm, and z = 10 µm, (b) CARS signal versus z.

3.5 Multimodal imaging of TPP structures

Finally, to demonstrate the capabilities of TRU, we carry out multimodal imaging of microstructures by three different techniques – TPF, CARS and THG. The microstructures are attached to a microscope slide, and they are fabricated by two-photon polymerization (TPP) [9] with the Newport Laser uFAB microfabrication workstation [10,11]. The powers and wavelengths used in the experiment, as well as the detection channels, are specified in Table 2:

The results are summarized in Fig. 7, which shows the TPF (a), CARS (b), THG (c), and scanning electron microscope (SEM, d) images of the same TPP structure. The collected images have 169 × 169 µm^2 size, and the signals are collected at a pixel dwell time of 12.5 µs, resulting in 3.3 s of scan time for each frame. The z-stack images are acquired in the range of z = –5 µm to z = 5 µm with a Δz = 0.5 µm step size. The insets show the brightest frames of z-stacks. The CARS (b) and THG (c) 3D images, along with the actual microstructure, also show a weak signal from the microscope slide within the 169 × 169 µm^2 imaging region. This is due to the CARS and THG signals from the glass, in contrast to the TPF image (a), where the glass contributes no TPF signal.

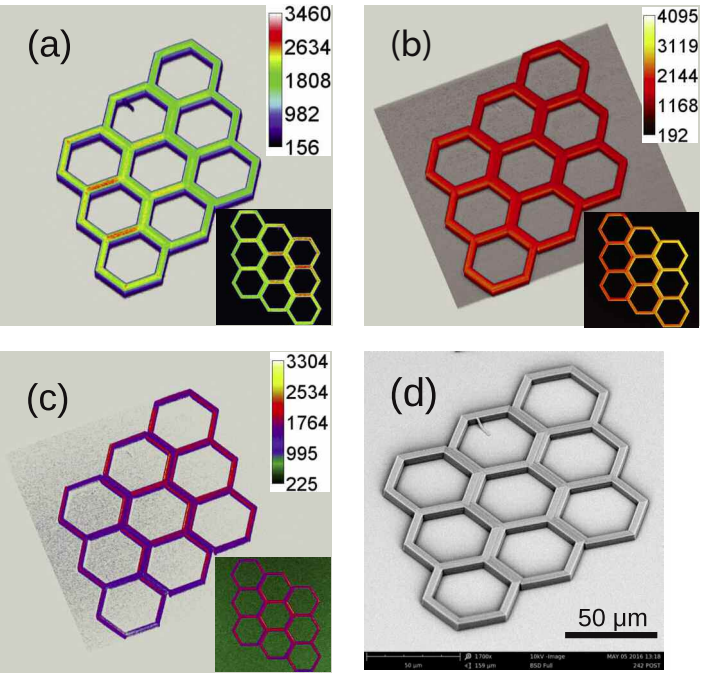

Fig. 7. Multimodal imaging of a TPP-fabricated microstructure: (a) TPF, (b) CARS, (c) THG, (d) SEM.

Table 2 – Experimental parameters

	Excitation wavelength(s) (nm)	Excitation power (mW)	Detection wavelength (nm)	Detection channel
TPF	800	5	520	epi
CARS	800 + 1041	5/each	650	forward
THG	1200	230	400	forward + epi

4. Conclusions

We have described a specially designed system TRU for dual wavelength, dual output laser sources, such as the Spectra-Physics InSight DS+ Dual. The performance and feasibility of TRU were demonstrated through experiments on time-resolved pump-probe spectroscopy, as well as CARS, THG and TPF microscopy imaging.

References

1. U. Keller, K. J. Weingarten, F. X. Kartner, D. Kopf, B. Braun, I. D. Jung, R. Fluck, C. Honninger, N. Matuschek, and J. Aus Der Au, "Semiconductor saturable absorber mirrors (SESAM's) for femtosecond to nanosecond pulse generation in solid-state lasers," IEEE J. Sel. Topics Quantum Electron. 2, 435–453 (1996).
2. W. Denk, J. H. Strickler, and W. W. Webb, "Two-photon laser scanning fluorescence microscopy," Science 248, 73–76 (1990).
3. P. Mahou, M. Zimmerley, K. Loulier, K. S. Matho, G. Labroille, X. Morin, W. Supatto, J. Livet, D. Débarre, and E. Beaurepaire, "Multicolor two-photon tissue imaging by wavelength mixing," Nat. Methods 9, 815–818 (2012).
4. N. G. Horton, K. Wang, D. Kobat, C. G. Clark, F. W.Wise, C. B. Schaffer, and C. Xu, "In vivo three-photon microscopy of subcortical structures within an intact mouse brain," Nat. Photon. 7, 205–209 (2013).
5. S. A. Akhmanov, N. I. Koroteev, A. I. Kholodnykh, "Excitation of the coherent optical phonons of Eg-type in calcite by means of the active spectroscopy method," J. Raman Spectrosc. 2, 239–248 (1974).
6. J.-X. Cheng and X. S. Xie, "Coherent anti-Stokes Raman scattering microscopy: instrumentation, theory, and applications," J. Phys. Chem. B 108, 827–840 (2004).
7. Y. Barad, H. Eisenberg, M. Horowitz, and Y. Silberberg, "Nonlinear scanning laser microscopy by third harmonic generation," Appl. Phys. Lett. 70, 922–924 (1997).
8. M. Muller, J. Squier, K. R. Wilson, and G. J. Brakenhoff, "3D microscopy of transparent objects using third-harmonic generation," J. Microsc. 191, 266–274 (1998).
9. T. Baldacchini and R. Zadoyan, "In situ and real time monitoring of two-photon polymerization using broadband coherent anti-Stokes Raman scattering microscopy," Opt. Express 18, 19219–19231 (2010).
10. Newport Corporation application note 37, "Three-dimensional microfabrication by two-photon polymerization" (Newport Corporation, 2008). https://www.newport.com/medias/sys_master/images/images/h26/hf7/8797287743518/Three-Dimensional-Microfabrication-App-Note-37.pdf
11. Newport Corporation application note 39, "Workstation for laser direct-write processing" (Newport Corporation, 2009). https://www.newport.com/medias/sys_master/images/images/h15/h4a/8797304651806/Workstation-for-Laser-Direct-Write-Processing-App-Note-39.pdf